Applying Mesh Conformation on Shape Analysis with Missing Data

Xiangyang Ju, Zhili Mao, J Paul Siebert
Department of Computing Science, University of Glasgow, UK
E-mail: {xju   jenny   psiebert}@dcs.gla.ac.uk

Nigel McFarlane, Jiahua Wu, Robin Tillett
Silsoe Research Institute, Silsoe, UK
E-mail: {nigel.mcfarlane jerry.wu robin.tillett }@bbsrc.ac.uk

Abstract

A mesh conformation approach that makes use of deformable generic meshes has been applied to establishing correspondences between 3D shapes with missing data. Given a group of shapes with correspondences, we can build up a statistical shape model by applying principal component analysis (PCA). The conformation at first globally maps the generic mesh to the 3D shape based on manually located corresponding landmarks, and then locally deforms the generic mesh to clone the 3D shape. The local deformation is constrained by minimizing the energy of an elastic model. An algorithm was also embedded in the conformation process to fill missing surface data of the shapes. Using synthetic data, we demonstrate that the conformation preserves the configuration of the generic mesh and hence it helps to establish good correspondences for shape analysis. Case studies of the principal component analysis of shapes were presented to illustrate the successes and advantages of our approach.

Keywords: dense 3D correspondence, conformation, 3D shape analysis, missing data.

1. Introduction

Abundant static/dynamic 3D surface/volume data have been acquired from various 3D imaging/scanning devices, such as C3D® photogrammetry stereo image system, Cyberware® Laser scanner, WWL® body scanner, MRI and CT. This leads to a requirement for 3D surface/volume modelling in many research areas, such as object recognition, image segmentation, 3D object retrieval, motion analysis, human body animation and medical diagnosis etc. The Point Distribution Model (PDM) [4] is one of the favourite approaches in shape modelling, which is based on the application of Principal Component Analysis (PCA) to a set of 3D shapes.

PCA requires that correspondences are established between the set of 3D shapes. Unfortunately, most imaging/scanning devices generate 3D data points that only implicitly represent shapes and as such do not afford any explicit semantic information. Due to the presence of self occlusions during the 3D acquisition process, or the effects of noise and outliers, the surface data recovered for an object or human subject is typically incomplete. In order to construct a Point Distribution Model (PDM), we have to somehow reconstruct the missing data and thereby establish a dense set of correspondences between the individual instances of our collection of 3D shapes.

Although there are many methods for filling holes in surfaces, most of these are piece-wise solutions. Carr *et al*. [3] used Radial Basis Functions (RBF) to reconstruct surfaces from point-cloud data and to repair incomplete meshes. An implicit surface was obtained as the zero-set of a RBF fitted to the given surface data. Lévy [9] made use of global parameterization of the surface to achieve surface hole-filling, surface fairing and blending, but it is only applicable if such a parameterization can be constructed. In this paper, we made use of our conformation process [6], [7] to fill missing data on a whole mesh, which represents a fundamentally different approach to that of the above global approaches.

Amongst the various approaches for establishing dense correspondences between 3D shapes, landmark based approaches [5], [10] with manual assistance can afford

certain advantages. In cases of large deformations between the shapes, or objects without significant features/curves, landmark based approaches have proven to be capable of reliably establishing dense correspondences [5]. We developed a conformation technique [6], [7] that made use of RBFs, initially for human body animation, which is similar to the method presented by Lorenz and Krahnstover [10]. Here, we apply this technique to establishing dense correspondences and filling missing data automatically on 3D surfaces which are not constrained to represent only the human form.

An elastic deformable model [12] was introduced to constrain both the conformation and missing data processes. It was believed that introducing the elastic model would cause the deformation to distribute more uniformly, so that the topological arrangement of the generic mesh could be better preserved [2], [13].

In this paper, we describe how we improved our conformation approach to maintaining correspondences between shapes via a deformable generic mesh and at the same time reconstructing missing data within the shapes globally. The method has the following properties:

- Correspondence between the shapes conformed is achieved through application of a global RBF mapping followed by local mesh optimization.
- The configuration of the generic mesh is predefined (i.e. tailored) according to requirements of shape analysis and the resolution of the mesh can be adjusted accordingly.
- Given a water tight generic mesh, the conformed mesh will also be water tight.

In section 2, we describe the details of the conformation process and an algorithm for reconstructing missing data. In section 3, firstly we present results of a test based on synthetic data to illustrate the effect of our elastic optimization. Secondly we demonstrate the reconstruction of missing data by taking advantage of the conformation process. Thirdly we present case studies of human body modelling and pig posture analysis. To conclude this paper (section 4), we indicate areas of potential future research based on the approaches presented.

2. Conformation

The conformation approach deforms a generic model to a desired shape by means of a two-step algorithm. The first step is a global mapping that brings the generic model close to the desired shape. The mapping uses Radial Basis Functions (RBF) [1], [3], [6], [7], [10] to interpolate the vertices of the generic mesh and is controlled by manually defined corresponding landmarks between the generic mesh and the desired shape. The second step relies on the first step and further deforms the generic model to the desired shape by deforming each vertex of the generic mesh to its most similar surface of the desired shape. Although the conformation deforms the generic model to the desired shape, it is naïve to deform the generic model in an unconstrained fashion. In our tests, a constraint has been adopted to prevent the generic mesh from either shrinking to a point or dilating excessively.

The generic mesh can be obtained either from 3D software packages, or 3D repositories, or one of the 3D shape samples can serve as a generic mesh directly.

2.1. Global Mapping

The predefined landmarks on the generic mesh and manually located landmarks on the scanned shape control the global mapping based on Radial Basis Functions (RBF).

Given N landmarks on the generic mesh $A=\{ \mathbf{a}_I, \ldots, \mathbf{a}_N \} \subset \mathbf{R}^3$ and corresponding landmarks on the scanned shape $S(A) = \{ \mathbf{s}_I, \ldots, \mathbf{s}_N \} \subset \mathbf{R}^3$, each vertex $\mathbf{x}$ of the generic mesh is mapped by $g(\mathbf{x})$ based on RBF

$$\mathbf{g}(\mathbf{x}) = \mathbf{p}(\mathbf{x}) + \sum_{i=1}^{N} \lambda_i \varphi(|\mathbf{x} - \mathbf{a}_i|), \mathbf{x} \in \mathbf{R}^3, \ i = 1,2,...,N \quad (1)$$

where $\mathbf{p}$ is an affine transformation, λ_i is a real-valued weight, φ is a basis function, $\varphi : \mathbf{R}^+ \rightarrow \mathbf{R}$, and $|\mathbf{x} - \mathbf{a}_i|$ is simply a distance. Here we select the biharmonic function $\varphi(r) = r$ as the basis function, where $r = |\mathbf{x} - \mathbf{a}_i|$.

2.2. Local optimized deformation

Following global mapping, the generic mesh is further deformed locally. The deformation of the generic model is constrained by minimizing the global energy of the generic mesh,

$$E = E_{ext} + \varepsilon E_{int} \quad (2)$$

where the parameter ε controls the trade-off between geometry similarity attractions and physical constraints. The external energy term attracts the vertices of the generic mesh to their most similar points on the scanned shape. It is defined as

$$E_{ext} = \sum_{i=1}^{n} w_i k_{ie} (\widetilde{\mathbf{x}}_i - \mathbf{x}_i)^2 \quad (3)$$

where n is the number of vertices on the generic mesh; k_{ie} is an external spring constant; $\mathbf{x}_i$ is the ith vertex; $\widetilde{\mathbf{x}}_i$ is its most similar point on the surface of the scanned object; w_i

is a weight related to the similarity between local surfaces patches of $\mathbf{x}_i$ and $\widetilde{\mathbf{x}}_i$. The internal energy term constrains the movement of the generic model and hence helps to maintain the original topology,

$$E_{\text{int}} = \sum_{i=1}^{n} \sum_{j=1}^{m} k_{ij} ((\mathbf{x}_i - \mathbf{x}_j) - (\bar{\mathbf{x}}_i - \bar{\mathbf{x}}_j))^2 \qquad (4)$$

where *m* is the number of neighbour vertices of the *ith* vertex, $\mathbf{x}_i$ and $\mathbf{x}_j$ are neighbouring vertices and $\bar{\mathbf{x}}_i$ and $\bar{\mathbf{x}}_j$ are their original positions in the generic mesh, k_{ij} is an internal spring constant. Since the energy function is quadratic with respect to $\mathbf{x}_i$, the optimization problem can be reduced to the solution of a sparse system of linear equations [8]. This linear system can be solved efficiently using the conjugate gradient method [11]. The positions of the vertices $\mathbf{x}_i$ are updated iteratively until the distances between $\mathbf{x}_i$ and $\widetilde{\mathbf{x}}_i$ are less than a tolerance.

2.3. Filling missing data

Object self-occlusion or the presence of noise and outliers within 3D imaging systems, typically results in an incomplete set of measurements being collected during 3D acquisition. We present an algorithm to reconstruct the missing data during the conformation process. This algorithm fills the missing data in a "grass fire" fashion (i.e. estimating data around the border of a hole until the hole is completely filled) and is embedded within the conformation iterative local optimization step.

Before local optimization deformation, each vertex of the generic mesh has to find its most similar point on the surface of the scanned model. If the vertex finds its similar point, the vertex is labelled with TRUE; otherwise it is labelled with FALSE. The algorithm for filling missing data is embedded into the conformation process as follows:

1. Map (based on the landmarks) the generic model to the surface of the scanned object.
2. Find the most similar $\widetilde{\mathbf{x}}_i$ on the surface of the object for all vertices $\mathbf{x}_i$ of the generic mesh, label each generic mesh vertex that finds a similar point with TRUE and label each generic mesh vertex for which no corresponding point could be found with FALSE.
3. Reconstruct the missing data
   a. Get one vertex labelled with FALSE.
   b. Find the neighbours of the vertex.
   c. If all its neighbours are labelled with FALSE, go to "a" get another vertex; otherwise set the displacement of the

vertex to the mean displacement of its neighbours labelled with TRUE; and then label it as TRUE.
   d. Repeat the steps "a" to "c" until no vertex labelled with FALSE.
4. After processing all vertices as above, calculate their optimal positions by minimizing the global energy of equation (2). Update the value of each $\mathbf{x}_i$ for the next iteration.
5. Repeat the steps 2 to 4 until the difference between $\mathbf{x}_i$ and $\widetilde{\mathbf{x}}_i$ is less than a tolerance.

3. Results

3.1 Effects of the optimization

To observe the effects of the optimization, the generic mesh statistics at the second stage of conformation were monitored, especially the variations of the lengths of edges and the variations of areas and angles of triangles. After each local optimization deformation, these variations were calculated by comparing the values of the original generic mesh with those of the deformed generic mesh. We believe that the low deviation values of the variations means that the deformation has been distributed across the mesh uniformly and that the topology of the mesh has been better preserved accordingly. A test based on synthetic data comprised conforming a sphere to a square where eight landmarks on the sphere were mapped to the eight corners of the square.
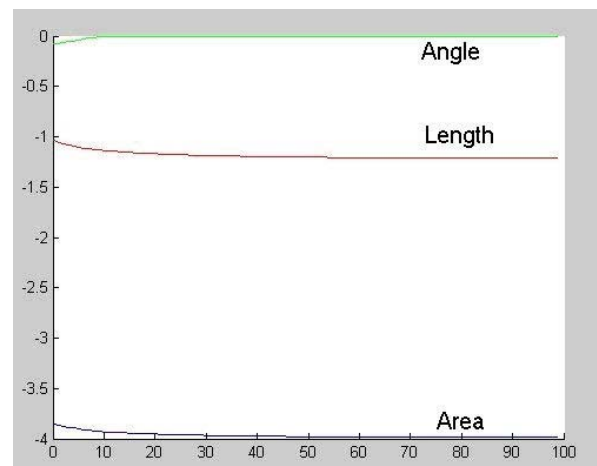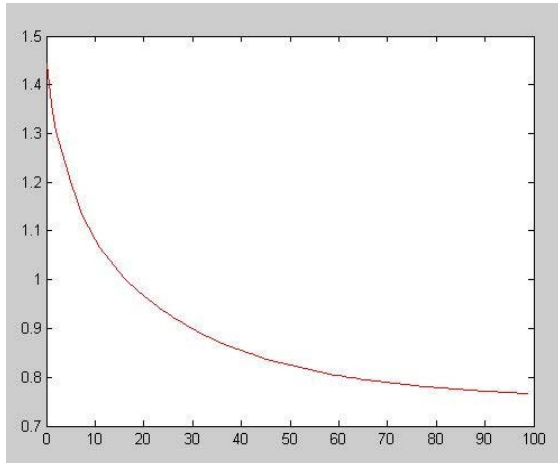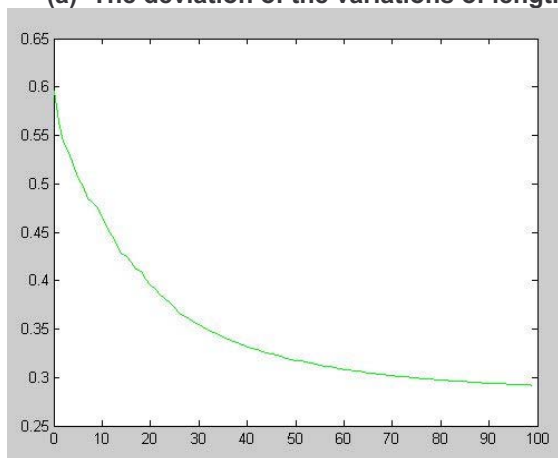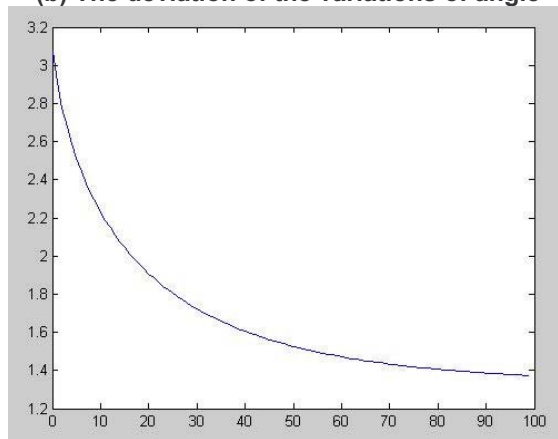

Figure 1. Mean variations of length, angle and area of triangles during each iteration

(a) The deviation of the variations of length

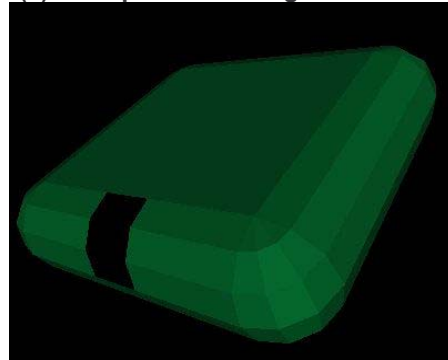**(b) The deviation of the variations of angle**

(c) The deviation of the variations of area

Figure 2. The changes of the deviations of the variations of the length, angle and area

In Figure 1, the mean variations of the lengths, angles and areas were nearly the same during the iterations, changing from -1.038 to -1.215, -0.079 to 0.000 and -3.854 to -3.988 respectively. The variations were plotted against the iteration times. The values of the means were not crucial here, while the trends of the mean values indicate that the mesh has changed locally.

(a) The sphere used a generic mesh
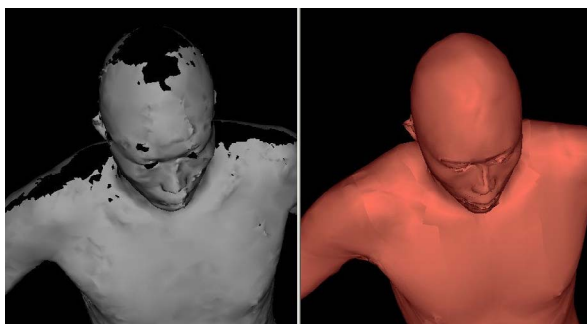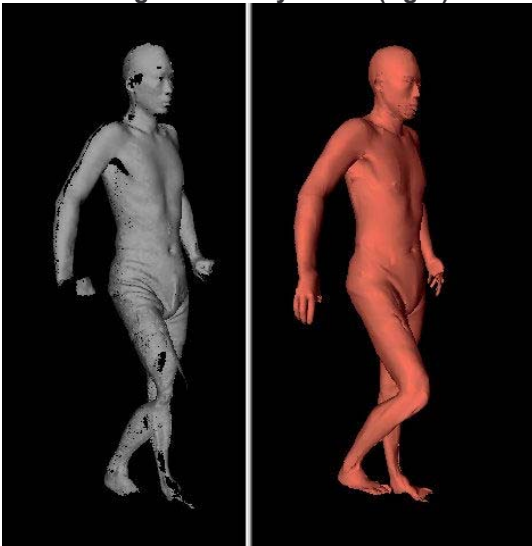

(b) A box with missing data
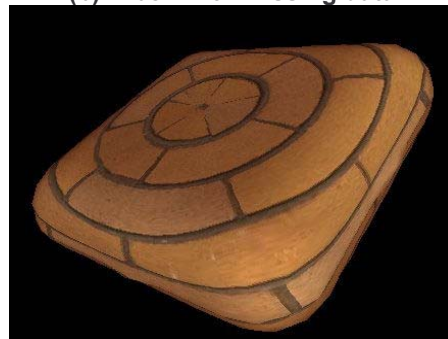
(c) Conformed result
Figure 3. A sphere (a) conformed into a box (b) results in (c)
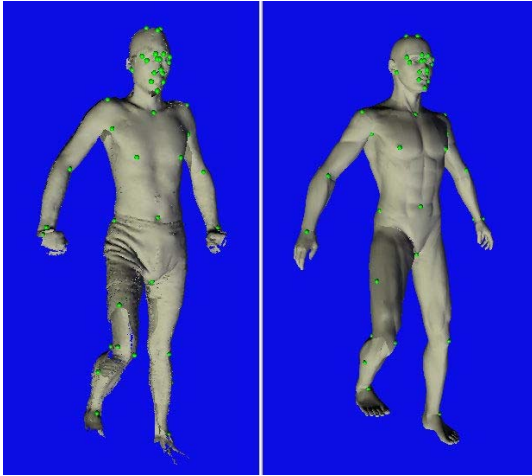
(a) Landmarks on the scanned shape (left) and the generic body model (right)

(b) Conformed generic mesh (right) comparing with the scanned shape (left)
Figure 4. Conformation of a human body

Furthermore, we calculated the deviations of the variations. In Figure 2, the deviation of the variations of the: edge lengths reduced from 1.52 to 0.78; the angles from 0.60 (34.5°) to 0.29 (16.6°) and; the areas from 3.07 to 1.37. The trends of the deviations demonstrated that the local optimization deformation tended to distribute the shape changes uniformly across the whole mesh.

3.2 Fill missing data

A second test using synthetic data comprised conforming a sphere to a box with missing data. Controlled by 6 landmarks, the sphere deformed into the exact shape of the box and the missing surface was reconstructed automatically.

An articulated generic mesh of a human body has been conformed to 50 different human body shapes obtained from a WWL® body scanner. Each conformation was controlled by 60 landmarks (Figure 4a). There were areas of missing data due to self occlusions during scanning. The conformed mesh demonstrated that the missing data could be reconstructed (Figure 4b). We noticed that a few areas of the generic mesh (ears, hands and feet) were severely distorted due to a lack of supporting surface data in these regions. This distortion could be prevented by setting a larger spring constant k_{ij} for the data corresponding to body parts which we do not want to change. Further investigation is required in this matter.

3.3 Shape Modelling

Equipped with the conformation tool for establishing dense correspondences between the shapes of scanned objects and reconstructing missing data automatically, we were able to construct a point distribution model. Figure 5 shows the mean of the 50 shapes.

Because of the articulation of the predefined generic body mesh, we were able to apply PCA to the segmented body as well as the whole body. Figure 6 shows the first three principal components of the torso, the mean shape of the torso being shown in the middle of each row. The mean shape superimposed with the negative/positive of each principal vector is shown in the left/right side of each row.

We have also undertaken the analysis of the postures of a pig using the techniques presented here. In this case the shapes of the pig at 12 postures were captured using our 3D photogrammetry imaging system. One of the 12 shapes was defined as the generic model, which was conformed into the other shapes of postures (Figure 7).
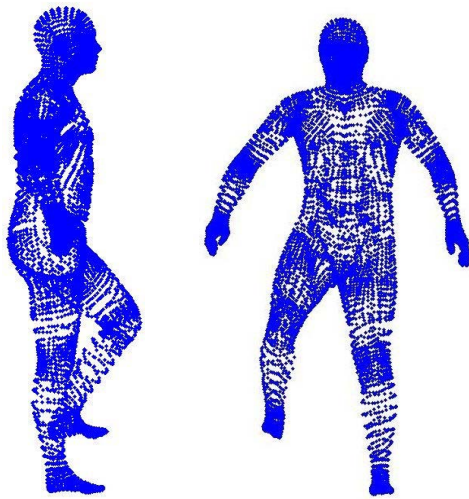
(a) Side view   (b) Front view
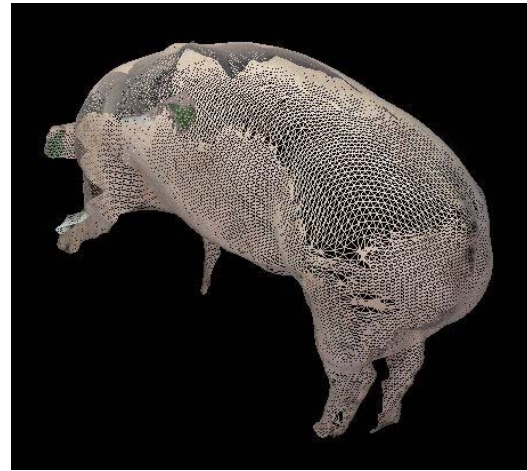Figure 5. Mean body shape
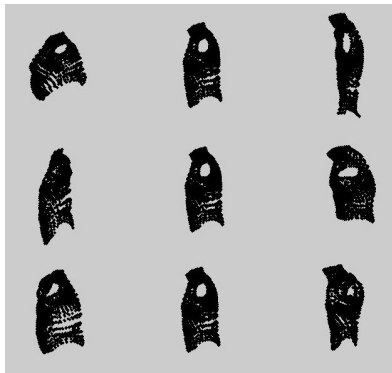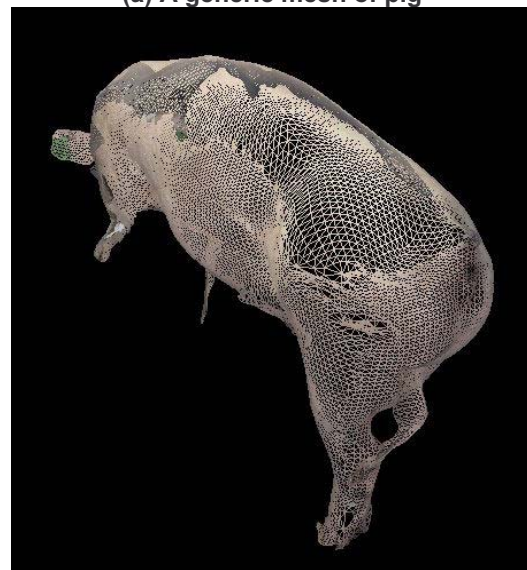

(a) Side view
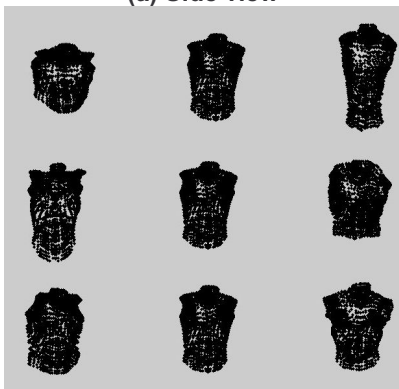
(b) Front view
Figure 6. Illustration of the first three principal
components of the torso

(a) A generic mesh of pig

(b) Conformed generic mesh to the shape
of another posture

Figure 7. The conformation of a generic
mesh of pig

The mean shape and the principal components were calculated and these are illustrated in Figure 8 and 9 respectively. The first component indicates that the dominant movement of the pig could be explained by the body swinging from left to right, and the second by the animal nodding its head. The third component indicates a twist of its body. Other components appear to be related to local movements.
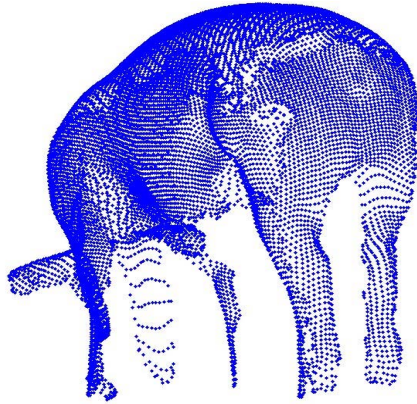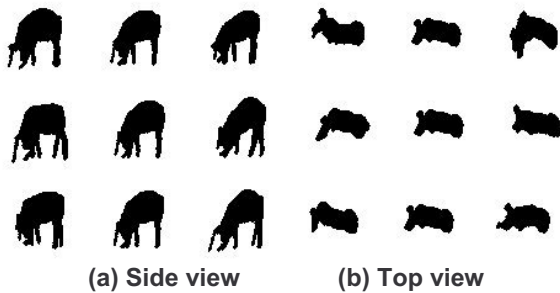
Figure 8. The mean shape of a pig at 12 postures

(a) Side view   (b) Top view
Figure 9. Illustration of the first three principal components

4. Conclusions and further work

We have demonstrated that we can successfully establish correspondences between shapes which have been synthetically generated or shapes which have been acquired using 3D imaging systems, while at the same time globally reconstructing missing data. Use of local optimization during mapping improved the quality of the resulting correspondences, as indicated by the trends of the deviations of the variations of the triangles comprising the generic mesh. The advantages of using our approach have been illustrated with two case studies. By using an articulated generic mesh for human body conformation, it becomes possible to segment the body into parts automatically and then analyse these shapes either globally or in isolation. During pig posture analysis, an instance of one of the shapes captures directly serves as the generic mesh to allow direct comparisons between "raw" datasets. Further work will include automated landmark detection and the usage of the spring constant as a means to control the adherence of the mesh to the underlying data.

References

[1] F. L. Bookstein, *Morphometric Tools for Landmark Data: Geometry & Biology*: Cambridge University Press, 1997.
[2] J. Brown, S. Sorkin, C. Bruyns, J. C. Latombe, K. Montgomery, and M. Stephanides, "Real-Time Simulation of Deformable Objects: Tools and Application," presented at *Computer Animation*, Seoul, Korea, 2001 November.
[3] J. C. Carr, R. K. Beatson, J. B. Cherrie, T. J. Mitchell, W. R. Fright, B. C. Mccallum, and T. R. Evans, "Reconstruction and representation of 3D objects with radial basis functions," presented at *ACM SIGGRAPH*, Los Angeles, CA, USA,, 2001, 12-17 August.
[4] T. F. Cootes, C. J. Taylor, D. H. Cooper, and J. Graham, "Active shape models- their training and application," *Computer Vision and Image Understanding*, vol. 61, pp. 38-59, 1995.
[5] T. J. Hutton, B. F. Buxton, and P. Hammond, "Dense Surface Point Distribution Models of the Human Face," presented at *Workshop Mathematical Methods in Biomedical Image Analysis* (MMBIA), Kauai, Hawaii, 2001 December.
[6] X. Ju and J. P. Siebert, "Conformation from generic animatable models to 3D scanned data," presented at *Proc. 6th Numerisation 3D/Scanning 2001 Congress*, Paris, France, 2001.
[7] X. Ju and J. P. Siebert, "Individualising Human Animation Models," presented at *Eurographics 2001 Short Presentation*, Manchester, UK, 2001.
[8] M. R. Kaus, V. Pekar, C. Lorenz, R. Truyen, S. Lobregt, and J. Weese, "Automated 3-D PDM construction from segmented images using deformable models," *IEEE Transactions on Medical Imaging*, vol. 22(8), pp. 1005-1013, 2003.
[9] B. Lévy, "Dual Domain Extrapolation", *ACM Transactions on Graphics* (TOG) archive, 22(3), Special issue: Proceedings of *ACM SIGGRAPH 2003*. pp. 364 – 369.
[10] C. Lorenz and N. Krahnstover, "Generation of Point-Based 3D Statistical Shape Models for Anatomical Objects," *Computer Vision and Image Understanding*, vol. 77, pp. 175-191, 2000.
[11] W. H. Press, S. A. Teukolsky, W. T. Vetterling, and B. P. Flannery, *Numerical Recipes in C++: The Art of Scientific Computing*, Cambridge university press, 2002.
[12] D. Terzopoulos, "Elastically deformable models," *Computer Graphics*, vol. 21(4), pp. 205-214, 1987 July.
[13] T. Vassilev, B. Spanlang, and Y. Chrysanthou, "Efficient Cloth Model and Collision Detection for Dressing Virtual People," presented at *Proc. GeTech*, Hong Kong, 2001 January.